# Mesh saliency with adaptive local patches

Anass Nouri, Christophe Charrier, Olivier Lézoray

# Mesh saliency with adaptive local patches

Anass Nouri, Christophe Charrier, Olivier Lézoray

Université de Caen, GREYC UMR CNRS 6072, Caen, France

## ABSTRACT

3D object shapes (represented by meshes) include both areas that attract the visual attention of human observers and others less or not attractive at all. This visual attention depends on the degree of saliency exposed by these areas. In this paper, we propose a technique for detecting salient regions in meshes. To do so, we define a local surface descriptor based on local patches of adaptive size and filled with a local height field. The saliency of mesh vertices is then defined as its degree measure with edges weights computed from adaptive patch similarities. Our approach is compared to the state-of-the-art and presents competitive results. A study evaluating the influence of the parameters establishing this approach is also carried out. The strength and the stability of our approach with respect to noise and simplication are also studied.

**Keywords:** Saliency, 3D Meshes, Graphs, Patches.

## 1. INTRODUCTION

A region of a 3D object is called salient if it is easily noticeable. There are two mechanisms in the human vision. The first process is called Bottom-Up. In this case, visual attention is involuntary focalized on specific regions of the 3D object and is related to the properties of the stimuli. The second one is called Top-Down process. In this case, the visual attention is focalized on what the observer looks for. We present in this work the saliency related to the Bottom-Up process which is called also Attentional Saliency. The salient regions in this case are content dependant and are not dependent of the behavior or the experience relative to the human observer[1] . Therefore, saliency computation can allow detecting perceptually imfportant points or regions on the surface of a 3D mesh. The saliency models proposed in the state-of-the-art are inspired from the HVS's (Human Visual System) low-level features. This allows to replace the geometrical attributes used for the computation of saliency by perceptual ones, and as confirmed in[2] , these perceptual models reach to model correctly the eye movement of the humain observer. Many applications in computer vision benefits from visual saliency, we can mention: optimal view point selection[3] where the objective is to generate the most informative viewpoints that capture a maximum of salient regions, adaptive mesh simplifcation[4] that aims at maintaining the best perceived quality by performing simplification essentially on regions of low saliency. Likewise, shape matching[5] , mesh resizing[6] , and face recognition[7] can take advantage from saliency detection.

## 2. STATE-OF-THE-ART

Unlike 2D images where saliency was amply dealt with (see[8] and references therein), there is few work on the evaluation of saliency directly on the geometry of the 3D meshes. For example, Lee et al.[3] proposed a model based on the computation of curvature[9] . For each vertex, they define a Gaussian-weighted average of the mean curvature. The saliency at a vertex is then the absolute difference between the gaussian weighted averages at both fine and coarse scales, respectively defined as $\sigma$ and $2\sigma$ (the band-with of the Gaussian filtering). The saliency is computed at different scales by varying $\sigma$. The final saliency is the aggregate of the saliency at all scales with a non-linear normalization.

Tal et al.[10] determine the surface regions of interest of a 3D mesh by taking into account the single-scale/multi-scale distinction and the presence of shape extremities. They use the Spin-Image histogram descriptor[11] to compute the dissimilarity between the vertices. This single-scale distinction permits the distinction of one vertex versus its neighbors. A vertex is distinct if its similar vertices are close to it and vice versa. Otherwise, the

Further author information: (Send correspondence to Anass Nouri.)
Anass Nouri: E-mail: anass.nouri@unicaen.fr, Telephone: +33231452712

multi-scale distinction is intended to reduce the influence of similar vertices that are apart from each other. For this, mesh faces are simplified. The multi-scale distinction is estimated by the mean distinction of the multiple scales. Finally the degree of interest of a vertex is defined by the maximum between its distinction and its degree of extremity.

In[12] , Jin Liang Wu et al. detect salient regions with a descriptor measuring the local height field into the neighborhood of each vertex; a square map[13] of projection heights is generated to denote its form. Then, Zernike moments are extracted from these maps to have a rotation invariant repsentation. Here, the multi-scale aspect of the descriptor is carried out by varying the size of the maps height. To first calculate the local saliency, the mesh is segmented into similar patches. The saliency of individual nodes is obtained by interpolating the saliencies of neighboring patches. Moreover, global saliency is assessed by grouping similar salient vertices into patches. Global saliency for each vertex is obtained by searching for the closer patches and interpolating their relative saliencies. Finally, the visual saliency of a vertex is computed by combining and normalizing the global and local saliency.

In[14] , Yitian et al. proposed a saliency detection method based on sampling for 3D mesh simplification. This approach begins by generating a saliency map in which perceptually important regions are located. The latter is then improved by Retinex theory based on characteristics of the human visual system. The realized mesh simplification taking into account the saliency map, is the result of transforming the 3D surface into volumetric data to select vertices belonging to each voxel according to saliency map entropy. To estimate this saliency map, a Gaussian filter is applied to the vertices. Then, parameters representing the mean curvature, and the principal curvatures are computed. For each couple of vertices, three saliency maps are generated according to the last computed parameters. These maps are filtered by a median filter before being combined to produce the final saliency map.

Acting on the same principle, the same authors Yitian et al. proposed in[15] a saliency model based on the index surface diffusion, likewise computed in[14] , but with a non-local filter[16] . This model was integrated in mesh registration and mesh simplification.

In[17] , Yitian and Liu detect salient regions by diffusing the surface index with a non local filter[16] . This time, the method is based on patches. The approach begins by filtering the mesh to delete high frequencies and compute similarities between vertices. Afterwards, the mesh is transformed into multi-scale volumetric data. The dissimilarity between two patches located in two sub-voxels allow to generate a dissimilarity map. Finally, the saliency of one patch, which is proportional to its dissimilarity, is defined by the average of the saliency maps across the different scales.

Song et al. suggested in[18] to integrate the CRF (Conditional Random Field) framework to detect saliency. This approach starts by generating a multi-scale representation of the mesh. This information is then combined using CRFs in order to label the mesh regions into salient and non-salient areas. The multi-scale representation is designed with a set of Gaussian filters applied on a neighborhood bounded by a geodesic raduis. The Difference-of-Gaussians (DoG) scale space is constructed and represents the displacement of vertices after the filtering operation. Then, the method incorporates the multi-scale information of a mesh into a Conditional Random Field (CRF) framework while introducing a consistency constraint between neighboring vertices to increase the robustness of the labeling approach. Finally to assign a label to each vertex, the CRF is resolved with the Belief Propagation algorithm.

In[19] , Y.Zhao et al. detect points of interest by estimating the saliency. The Retinex theory[20] is implemented to enhance the local details and estimate the invariant properties of the surface views. After the segmentation of the surface, the saliency is estimated based on the spatial distance between the resulting segments.

Recently, Song et al. suggested in[21] to estimate the saliency in the spectral domain by analyzing the irregularity spectrum of the Log-Laplace operator that is bounded to the saliency according to the authors. First, the spectrum of the Laplacian is calculated, then a logarithmic transformation is applied to the spectrum to amplify variations at low frequencies while removing them from the rest of the spectrum. These deviations represent saliency. The aim of this approach is to detect changes in the spectrum, and calculate the spectral deviation. The latter is then calculated in the spatial domain as a matrix wherein the sum of each row represents the saliency of a node. In this method, the saliency of a triangular mesh is estimated by applying the above method

on two versions of the mesh generated from the original. The first is provided by filtering the simplified mesh with a Gaussian filter, the second is computed using dynamic scales. Next, the saliency maps are calculated by the absolute difference between the estimated saliency on both simplified versions. Finally, the saliency maps are mapped to the original mesh, and summed to have the saliency map at a target vertex. The resulting map is smoothed to derive the final saliency map.

### 2.1 Contributions

As described above, most of existing approaches estimating 3D mesh saliency include a simplification step in their process to define a good ratio between Sailency and Noise that is sometimes difficult to define. This simplification step inevitably removes vertices from the mesh geometry and therefore alters the surface and its initial fluctuations. The result is then a measure of saliency that does not take into account local variations and exiguous irregularities, yet necessary for the accurate estimation of saliency on surface meshes. Other steps such as smoothing bring back to a very high complexity.

It is commonly accepted that the human visual system is sensitive to large fluctuations surfaces[22] . Thereby, if a mesh vertex stands out strongly from its neighborhood, then this vertex could be considered as salient point. It remains to define the way in which we can locally evaluate the saliency of a vertex within the mesh. For this, local robust descriptors are carried out.

In this paper we propose a new method to define a perceptual saliency map for 3D meshes.

Our approach differs from other methods by using adaptive patches for better local representation of the surface and therefore for a better detection of salient areas. The saliency in our case is defined by the degree of each vertex. This degree will be calculated from the similarities, which benefit from a scale parameter, between the 2D patches of the target vertex and its neighboring vertices. Also note that our approach is independent of any pre-treatment like simplification or smoothing. This autonomy will allow fitting this approach into any mesh processing algorithm. All these factors lead to an accurate estimation of visual saliency.

## 3. MESH SALIENCY

### 3.1 Modeling the surface

In order to define the local descriptors of a surface mesh, it is necessary to model the surface to be treat. To do so, we represent a mesh M by an undirected graph $G = (V, E, w)$ where $V$ represents the set of vertices, $E \subset V \times V$ the set of edges, and $w(v_i, v_j)$ the weight of the edge $(v_i, v_j) \in E$.

For every vertex $v_i$ on the mesh surface, we compute its normal vector $\vec{z}(v_i)$ and the directional vectors $\vec{x}(v_i)$ and $\vec{y}(v_i)$ that correspond to the estimation of the 2D tangent plan at vertex $v_i$ on the mesh. We denote $v_j \sim v_i$ if $\exists(v_j, v_i) \in E$ and $N(v_i) = \{v_j | v_j \sim v_i\}$ . In the first step, we compute the cardinality of the direct neighborhood of $v_i$ $|N(v_j)|$ in order to calculate the center of gravity $\hat{v_i}$ as:

$$\hat{v_i} = \frac{1}{|N(v_i)|} \sum_{j \in N(v_i)} v_j \tag{1}$$

together with the associated covariance matrix at $v_i$ defined as:

$$cov(v_i) = \sum_{j \in N(v_i)} (v_j - \hat{v_i})(v_j - \hat{v_i})^T \in \mathbb{R}^{3\times 3} \tag{2}$$

We will use the eigen-values of the covariance matrix to determine both the normal vector $\vec{z}(v_i)$ and the 2-directional vectors following the x and y axes.

Thus, the mesh surface will be represented by vertices with their respective normals and tangent planes. However the normal vectors can have different directions (outwards and inwards). To guide these normals outwards, we propagate the orientation of the neighboring normals using the minimum spanning tree of the graph[23] .

### 3.2 Local adaptive patches construction

Once the mesh has been modeled by the procedure described above, we build the local adaptive patches to describe the vertices local surfaces. First, the nodes contained in a sphere $S_\varepsilon(v_i) = \left\{v_j \mid ||\vec{v_j} - \vec{v_i}||_2^2 \leq \varepsilon\right\}$ centered at $v_i$ within a radius $\varepsilon$ are considered. They are projected onto the 2D plan $\vec{P}(v_i)$ defined by the associated vectors. It follows from this 2D projected vectors $\vec{v_j'}$:

$$\vec{v_j'} = [(\vec{v_j} - \vec{v_i}) \cdot \vec{x}(v_i), (\vec{v_j} - \vec{v_i}) \cdot \vec{y}(v_i)]^T \tag{3}$$

Then it remains to define the size of the patch. We propose a dynamic configuration based on the distance between the 2D coordinates of the projected vertices from the sphere $S_\varepsilon$. Indeed it is possible to define the dimensions of the patch according to the abscissa and ordinate axis (respectively denoted $T_x(.)$ and $T_y(.)$) by:

$$\mathrm{T}_d(v_i) = \max_{(\vec{v_j'}, \vec{v_k'}) \in \vec{P}(v_i)} (||\vec{v_j'^d} - \vec{v_k'^d}||_2^2) \tag{4}$$

where $d$ represents the $x$ or $y$ coordinates, $v_j'^d$ the $d$ coordinate of $\vec{v_j'}$, and $||.||_2$ the Euclidean norm.

Thus, the patch at vertex $v_i$ is represented by a rectangle of size $\mathrm{T}_x(v_i) \times \mathrm{T}_y(v_i)$ centered at $v_i$. It should be noted that usually a patch is represented by a square of fixed size and does not allow to get an adaptative local descriptor depending on the local geometry. This local patch is then divided into $l \times l$ cells in order to specify the index of the cell in which a neighboring vertex will be projected:

$$\mathrm{index}^d = \left\lfloor \frac{\vec{v_j'}^d}{\mathrm{T}_d(v_i)/l} \right\rfloor \text{ with } v_j \sim v_i \tag{5}$$

where $v_j \sim v_i$ denotes two adjacent vertices in the mesh and $\lfloor \cdot \rfloor$ denotes the integer rounded.

Finally, each cell of the patch is filled with the absolute value of the sum of the projections heights:

$$\mathrm{H}(\vec{v_j'}) = ||(\vec{v_j} - \vec{v_j'})||_2^2 \tag{6}$$

Figure 1 illustrates the construction of patches.

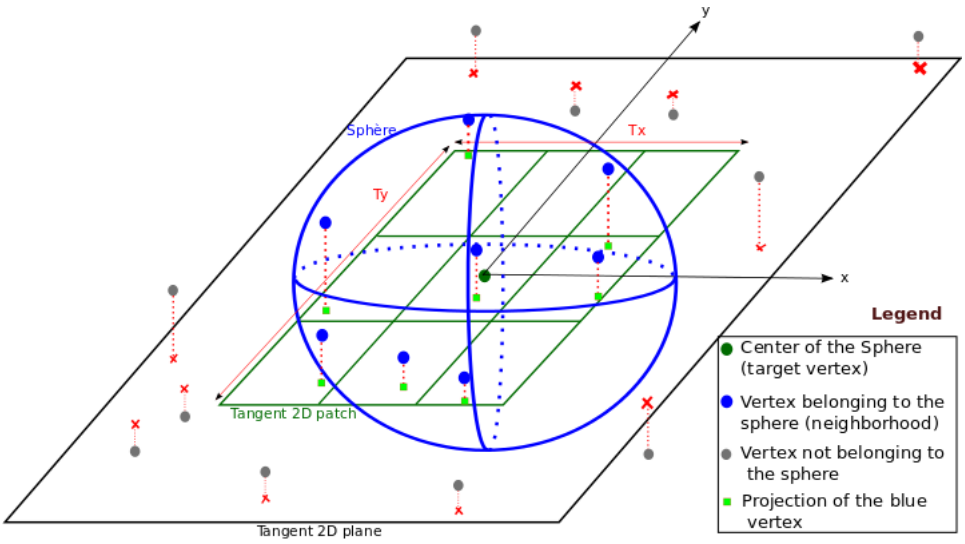


Figure 1. Illustration of the adaptive patch construction

It is important to note that the adaptive size of patches is not related to the radius $\varepsilon$ of the sphere, but instead to the maximum distance between the 2D projections of the vertices along the x axis in one hand, and the y axis in the other hand. This enforces its adaptive aspect.

This method of patch construction also works for 3D points cloud instead of 3D meshes as the mesh-topology is not taken into account but only the set of points in a $\varepsilon$-ball.

### 3.3 Saliency computation

To compute the saliency of a vertex, a measure of similarity between its associated patch and the patches associated to its neighbors is required. We propose to locally compute a scale parameter (standard deviation of Gaussian kernel measuring the dissimilarity). Indeed, using a specific scale parameter for each node allows us to take into account the local distribution around each grid node.
The scale parameter $\sigma(v_i)$ is then determined by:

$$\sigma(v_i) = \max_{v_k \sim v_i} (||\vec{v_i} - \vec{v_k}||_2) \tag{7}$$

Note that we have tested the scale parameter based on the difference between the vectors of accumulated heights (see below) and it has been found that the difference between 3D coordinates vertices leads to better results.

Thus, the similarity is assigned to the weight of the edge $(v_i, v_j)$ is:

$$\mathrm{w}(v_i, v_j) = \exp\left[-\frac{||\vec{H}(v_i) - \vec{H}(v_j)||_2^2}{\sigma(v_i) * \sigma(v_j)}\right] \text{ with } v_j \sim v_i \tag{8}$$

where $\vec{H}(v_i) \in \mathbb{R}^{l \times l}$ is the vector of accumulated heights into the cells of the patch and $||.||_2^2$ represents the Euclidean distance.

Finally, the visual saliency of the vertex $v_i$ on the 3D mesh is defined by its degree as:

$$\text{Saliency}(v_i) = \left(\frac{1}{|N(v_i)|}\right) \sum_{v_i \sim v_j} w(v_i, v_j) \tag{9}$$

where $w(v_i, v_j)$ is the weight of the edge between vertices $v_i$ and $v_j$ and $|N(v_i)|$ is the cardinality of the neighboring.

## 4. THE INFLUENTIAL PARAMETERS

Two parameters affect the rendering of the saliency: the number of patch cells $l$ and the radius of the sphere $S_\varepsilon$ containing the vertices to be projected. Table 1 presents the amplitude of the detected saliency according to the $l$ and $\varepsilon$ parameters.

We can notice on Table 1 that saliency depends strongly on both the neighborhood delimited by the sphere $S_\varepsilon$ and the number of cells of the adaptative patch. In Table 1, a radius equal to 1 provides the detection of very small salient details. Also note that in this case, increasing the number of cells does not affect the estimate of saliency. In contrast, a sphere of radius equal to 4 greatly expands the neighborhood, which brings to an extreme description of the mesh surface, and thus taking into account the extreme fluctuations on the surface which brings to detect the large salient regions. We can also notice that the number of salient points increases proportionally to the number of cells. These 3 radii of the sphere $S_\varepsilon$ may permit to design a multi-scale saliency on our future works.

Table 1. Influence of parameters $\varepsilon$ and $l$ on the detection of saliency.

| | Number of cells $l$ | | |
|---|---|---|---|
| | 7x7 | 17x17 | 27x27 |
| $\varepsilon$=1 | 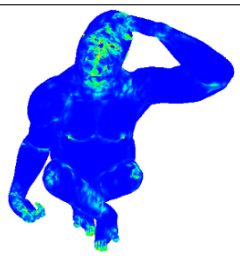 | 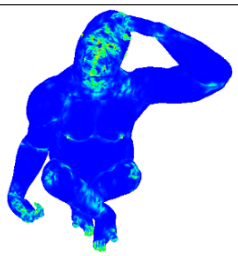 | 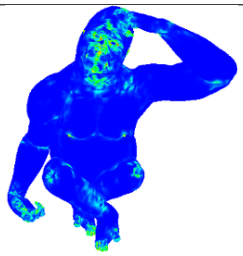 |
| $\varepsilon = 2$ | 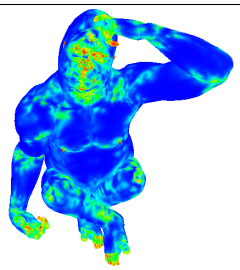 | 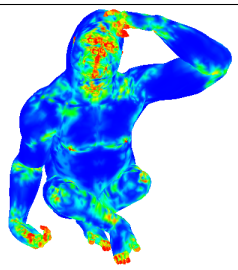 | 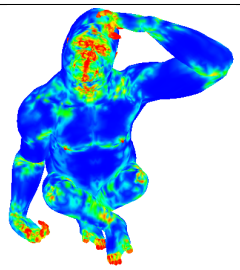 |
| $\varepsilon$=4 | 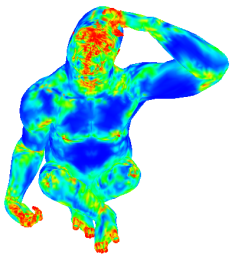 | 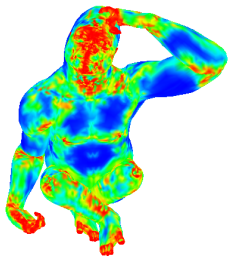 | 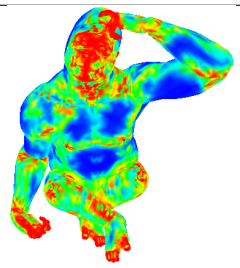 |

## 5. RESULTS AND ANALYSIS

Figure 2 presents the saliency estimated by our approach on the 3D object Gorilla (Figure 2(a)). Figure 2(b) shows that our method brings out finely the salient regions on the 3D mesh surface. Figure 2(c) shows a zoom on the face of the 3D object Gorilla. One can see that the smallest details such as eyes, mouth, nose, and ears are finely put forward.

Figure 3 shows a comparison of the detected saliency on the 3D object Dinosaur with the state-of-the-art. As outlined above, our approach considers out-standing vertices (in relief) in a flat surface as salient points (discontinuities on surfaces naturally attract the attention of the human observer). Tal et al.'s approach[10] judges the ribs of the 3D Dinosaur model located on the back and the stomach as non-salient regions (Figure 3(c)). Yet, these areas fluctuate enormously and contain high discontinuities in the surface (see the zoom figure 4). In Figure 3(b), our method assesses ribs of the object Dinosaur as salient regions given their high discontinuities, and contrary to the approach of[10] Figure 3(c), the relative area of skull (except the eye and some curvatures) is not considered as a completely salient region. This also means that at the first glance in the direction of the object Dinosaur, visual attention will be placed firstly on a part of the fluctuating ribs or the neck, rather than on the surface of its skull. In Figure 3(d)[3] , we can notice again that the saliency on the ribs is weakly detected (colored in light green). Locally finest details are not taken into account, contrary to our approach. However, in Figure 3, Song et al.'s approach[21] has a similar saliency as ours. It can differentiate between areas with high discontinuities and flat ones.

Figure 5 shows a comparison of the estimated saliency on the 3D mesh Angel by the approaches[10] and[21] . 3D object Angel's surface is complex as it contains many extremities. It has also both rough and smooth surfaces.

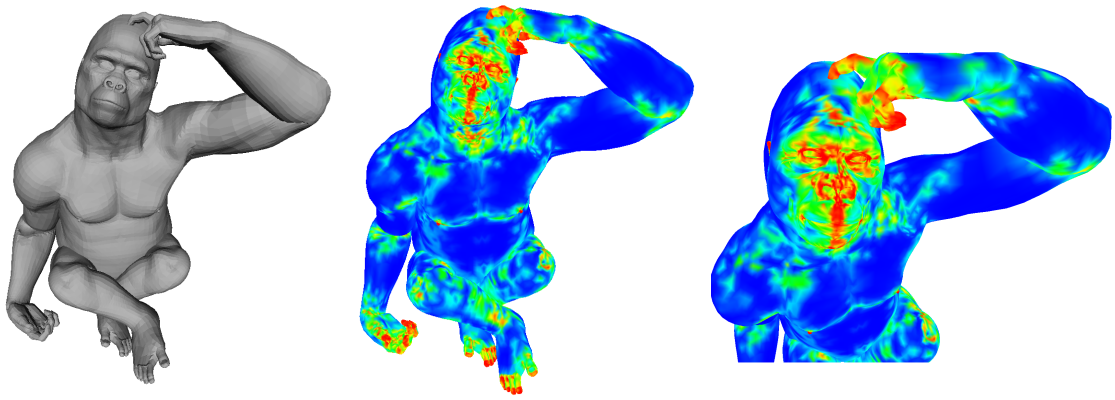

(a) (b) (c)

Figure 2. Saliency by our approach: image (a) shows the original 3D object Gorilla (25 438 vertices), image (b) shows its saliency by our method ($\varepsilon = 2$ and $l = 17$) and image (c) shows a zoom on the saliency detected on the face of the gorilla object.

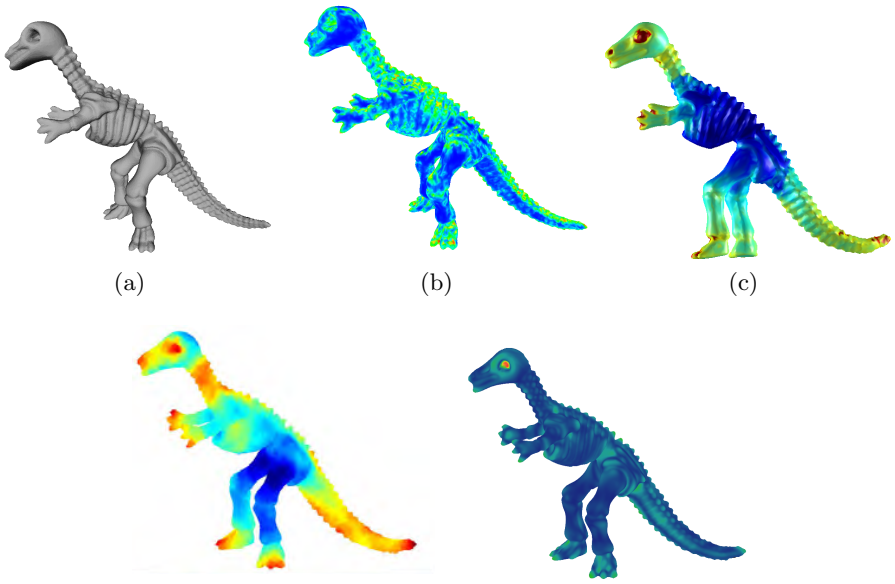

(a) (b) (c)

(d) (e)

Figure 3. Comparison with the state-of-the-art: image (a) shows the original 3D object dinosaur (21 777 vertices), image (b) shows its saliency by our method ($\varepsilon = 0.013$ and $l$=17), image (c) shows the saliency detected by the approach of[10] , image (d) shows the saliency detected by the approach of[21] and image (e) shows the saliency detected by the approach of[3] .

One can see that the extremity of the scarf presents a lot of fluctuations. This one is considered salient by the approach of[21] and ours while the approach of[10] considers it as non salient. The discontinuities on the eyes, the arms, the hip and the stomach are represented as salient by the approach of[21] and ours, contrary to the method of[10] .

Figure 6 compares the salient regions estimated on the 3D object horse by our approach and those estimated by approaches of[10] and[21] . We can notice that our method and the method of[21] are able to detect the eyes, highly regarded parts in scenes or objets containing faces[24] , and judge them as very salient regions while the approach of[10] fails in this regard. The horse's back has muscled parts like the Centaur object (Figure 7). These areas are also assessed as salient regions by our approach and the approach of[21] contrary to the approach of[10] .

Figure 7 presents the saliency detected on other 3D objects. We can notice the same behavior of our method,

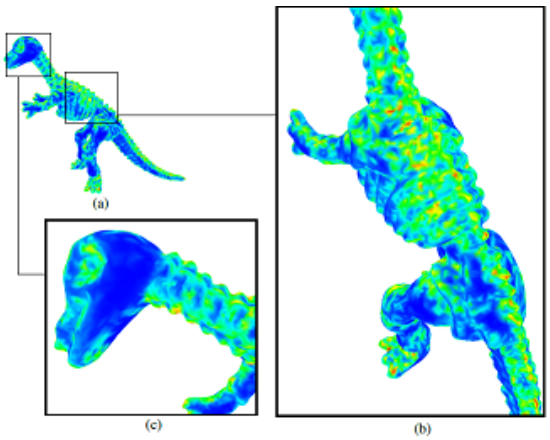


Figure 4. Zoom on exiguous details of the 3D object Dinosaur: (a) Saliency of the Dinosaur estimated by our approach, (b) Zoom on the saliency related to the ribs of the Dinosaur, (c) Zoom on the skull of the object Dinosaur.

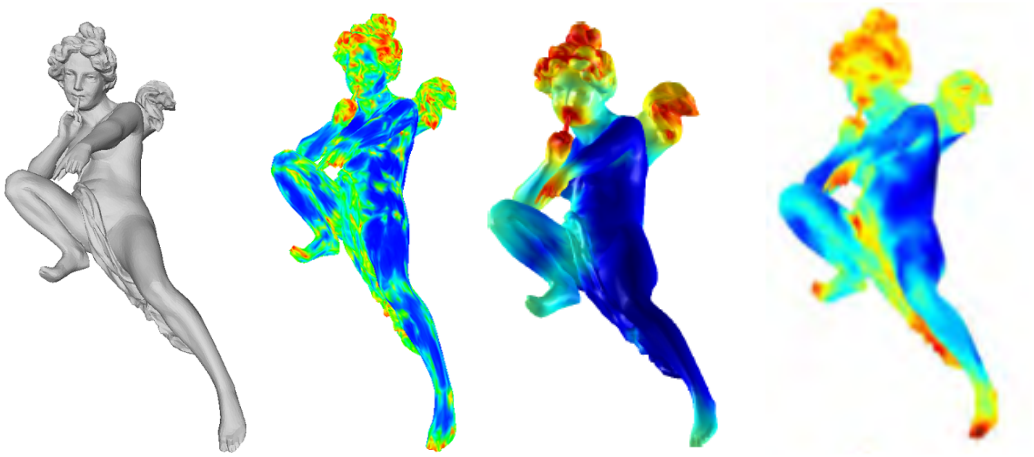

(a) (b) (c) (d)

Figure 5. Comparison with the state of the art: image (a) shows the original 3D object Angel (14227 vertices), image (b) shows its saliency by our method ($l$=27), image (c) shows the saliency detected by the approach of[10] and image (d) shows the saliency detected by the approach of[21] .

which allows a precise estimate of the saliency.

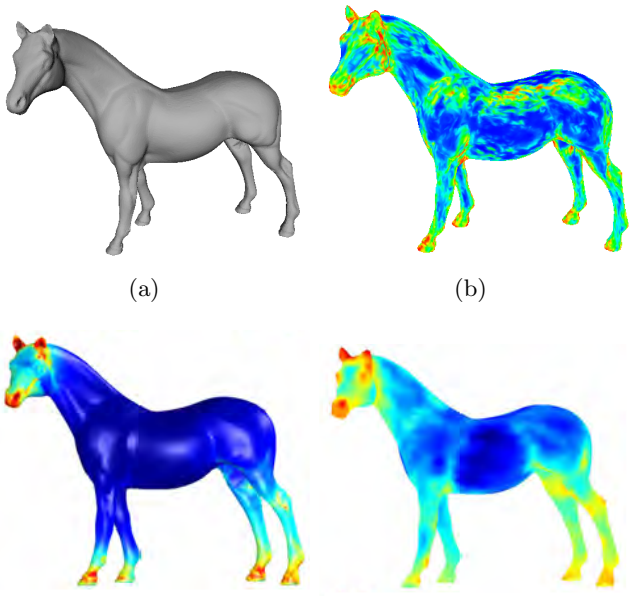

(a) (b) (c) (d)

Figure 6. Comparison with the state-of-the-art: image (a) shows the original 3D object Horse (20 871vertices), image (b) shows its saliency by our method ($\varepsilon = 0.4$ and $l$=17), image (c) shows the saliency detected by the approach of[10] and image (d) shows the saliency detected by the approach of[21] .

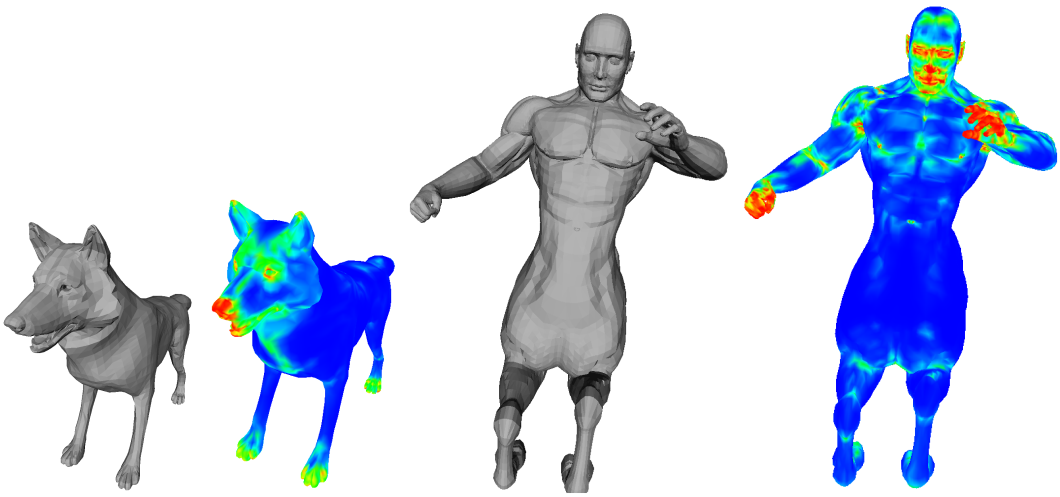

(a) (b) (c) (d)

Figure 7. Saliency detected on different 3D objects : image (a) shows the original 3D object Wolf (4 344 vertices), image (b) shows its saliency by our approach ($\varepsilon = 3$ and $l = 27$), image (c) shows the original 3D object Centaur (15 768 vertices) and image (d) shows its saliency estimated by our approach ($\varepsilon = 2.5$ and $l = 27$).

## 6. ROBUSTNESS

To attest the robustness of our approach, we put noise on the 3D mesh Centaur by randomly displacing the positions of its vertices according to 3 levels of noise. Then, we applied our multi-scale saliency measure.

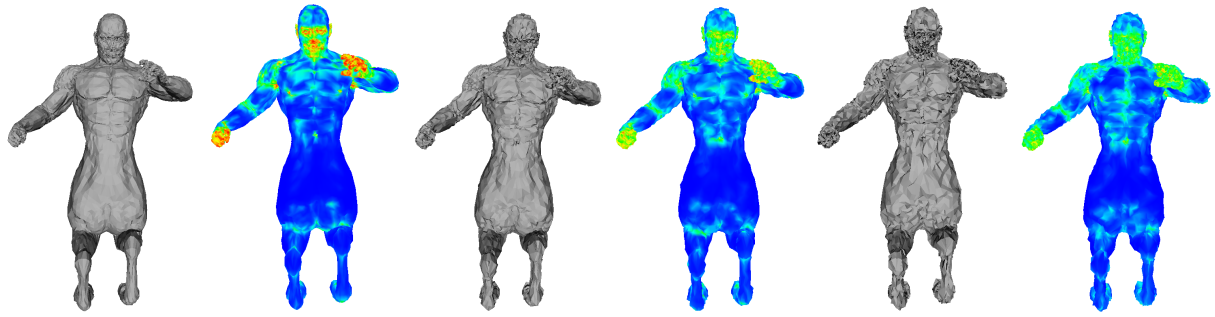

(a) (b) (c) (d) (e) (f)

Figure 8. Robustness to noise: image (a) shows the original 3D object Centaur noised (displacement= -0.1%), image (b) shows the saliency of the Centaur noised with -0.1%, image (c) shows the original 3D object Centaur noised (displacement= -0.2%), image (d) shows the saliency of the Centaur noised with -0.2%, image (e) shows the original 3D object Centaur noised (displacement= -0.3%) and image (d) shows the saliency of the Centaur noised with -0.3%. Note how the original salient regions still remain salient despite the sever noise.

Figure 8 shows that visually, our method always succeeds to detect the same salient regions despite the fact that the mesh surface was severely noised. Areas like the eyes, the mouth, the nose, the paws still are considered salient and can be differentiated from the other flat regions.

Another experiment that demonstrate the stability of our method is measuring saliency on simplified meshes. Simplification was operated using Garland et al's algorithm[25] .

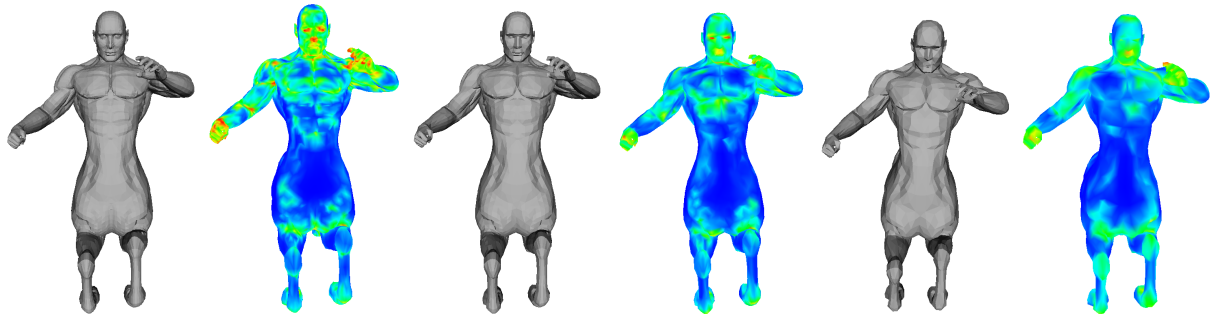

(a) (b) (c) (d) (e) (f)

Figure 9. Robustness to simplification: image (a) shows the original 3D object Centaur simplified to 37.5% (9885 vertices), image (b) shows the saliency of the Centaur simplified to 37.5% (9885 vertices), image (c) shows the original 3D object Centaur simplified to 68.3% (4 947 vertices), image (d) shows the saliency of the Centaur simplified to 68.3% (4 947 vertices), image (e) shows the original 3D object Centaur simplified to 79.5% (3 147 vertices) and image (f) shows the saliency of the Centaur simplified to 79.5% (3 147 vertices).

In figure 9(a), the mesh is simplified to 37.5% (37.5% of the initial vertices were deleted) and we can notice that the initial salient regions still are detected (figure 9(b)). The same result can be observed in figure 9(d). In figure 9(e), the mesh is simplified to 79.5%. The same regions are still put forward but with less intensity (figure 9(f)). This is due to the strong simplification that tends to delete the discontinuities and therefore flattens the vertices. Flat surfaces present naturally a low visual saliency.

## 7. COMPLEXITY ANALYSIS

The complexity of calculating normals depends on the number of neighbors $k$ that the target vertex has. To compute the global complexity, k is increased by the maximum number of neighbors $\max_{v_i}(|N(v_i)|)$. Thus, the complexity of calculating normals is $O(|V|k)$. The orientation of normals using the minimum spanning tree of

the graph has a complexity of $O(|V|log|V| + |E|)$. Building the local adaptive patches and calculating saliency are both related to the neighboring of the target vertex, they have a complexity of $O(|V|k)$. Finally, the global saliency of the proposed approach is :

$$O(|V|k) + O(|V|log|V|| + |E|) \tag{10}$$

**Speed :** For the Gorilla mesh that contains 25 438 vertices and 152 616 edges, the execution time to measure saliency with $\varepsilon = 2$ et $l = 17$ (for a non optimized implementation) is 85s.

## 8. CONCLUSION

We have presented a method for detecting salient regions on 3D meshes. Our method considers only the geometry of the 3D mesh and is independent of any pretreatment like simplification or smoothing. The descriptors that encode the irregularities of the mesh surface are based on the projection of prominent vertices (that stand out from a local neighborhood on the surface) on local adaptive patches. The adaptive size of the patches leads to a better consideration of the exiguous discontinuities that attract visual attention. Afterward, a similarity measure between patches leads to quantify the perceptual saliency of a vertex relative to another, and then to obtain the saliency at each vertex of the mesh.
Future works will aim at improving the saliency map by considering the hierarchical aspect of the human vision and by integrating new perceptual attributes in measuring the degree of vertices that express saliency.

## REFERENCES


1. L. Itti, C. Koch, and E. Niebur, "A model of saliency-based visual attention for rapid scene analysis," *IEEE Trans. Pattern Anal. Mach. Intell.* **20**(11), pp. 1254–1259, 1998.
2. Y. Kim, A. Varshney, D. W. Jacobs, and F. Guimbretière, "Mesh saliency and human eye fixations," *ACM Trans. Appl. Percept.* **7**(2), pp. 12:1–12:13, 2010.
3. C. Lee, A. Varshney, and D. W. Jacobs, "Mesh saliency," *ACM Trans. Graph.* **24**(3), pp. 659–666, 2005.
4. P. Shilane and T. Funkhouser, "Distinctive regions of 3D surfaces," *ACM Trans. Graph.* **26**(2), 2007.
5. R. Gal and D. Cohen-Or, "Salient geometric features for partial shape matching and similarity," *ACM Trans. Graph.* **25**(1).
6. S. Jia, C. Zhang, X. Li, and Y. Zhou, "Mesh resizing based on hierarchical saliency detection," *Graph. Models* **76**(5), pp. 355–362, 2014.
7. L. Jinho, M. Baback, P. Hanspeter, and M. R. Machiraju, "Finding optimal views for 3D face shape modeling," in *Proc. International Conference on Automatic Face and Gesture Recognition*, pp. 31–36, 2004.
8. Z. Liu, W. Zou, and O. Le Meur, "A novel saliency detection framework," *Image Processing, IEEE Transactions* **23**, pp. 1937 – 1952, Feb. 2014.
9. G. Taubin, "Estimating the tensor of curvature of a surface from a polyhedral approximation," in *Proceedings of the Fifth International Conference on Computer Vision*, *ICCV '95*, pp. 902–, IEEE Computer Society, (Washington, DC, USA), 1995.
10. A. Tal, E. Shtrom, and G. Leifman, "Surface regions of interest for viewpoint selection," *2013 IEEE Conference on Computer Vision and Pattern Recognition* , pp. 414–421, 2012.
11. A. E. Johnson and M. Hebert, "Using spin images for efficient object recognition in cluttered 3d scenes," *IEEE Trans. Pattern Anal. Mach. Intell.* **21**(5), pp. 433–449, 1999.
12. J. Wu, X. Shen, W. Zhu, and L. Liu, "Mesh saliency with global rarity," *Graph. Models* **75**(5), pp. 255–264, 2013.
13. A. Maximo, R. Patro, A. Varshney, and R. Farias, "A robust and rotationally invariant local surface descriptor with applications to non-local mesh processing," *Graph. Models* **73**(5), 2011.
14. Y. Zhao, Y. Liu, R. Song, and M. Zhang, "A saliency detection based method for 3d surface simplification," in *2012 IEEE International Conference on Acoustics, Speech and Signal Processing, ICASSP 2012, Kyoto, Japan, March 25-30, 2012*, pp. 889–892, 2012.

15. Y. Zhao, Y. Liu, R. Song, and M. Zhang, "Extended non-local means filter for surface saliency detection," in *19th IEEE International Conference on Image Processing, ICIP 2012, Lake Buena Vista, Orlando, FL, USA, September 30 - October 3, 2012*, pp. 633–636, 2012.
16. A. Buades, B. Coll, and J.-M. Morel, "A non-local algorithm for image denoising," in *Proceedings of the 2005 IEEE Computer Society Conference on Computer Vision and Pattern Recognition (CVPR'05) - Volume 2 - Volume 02*, *CVPR '05*, pp. 60–65, IEEE Computer Society, (Washington, DC, USA), 2005.
17. Y. Zhao and Y. Liu, "Patch based saliency detection method for 3d surface simplification," in *Proceedings of the 21st International Conference on Pattern Recognition, ICPR 2012, Tsukuba, Japan, November 11-15, 2012*, pp. 845–848, 2012.
18. R. Song, Y. Liu, Y. Zhao, R. R. Martin, and P. L. Rosin, "Conditional random field-based mesh saliency," in *19th IEEE International Conference on Image Processing, ICIP 2012, Lake Buena Vista, Orlando, FL, USA, September 30 - October 3, 2012*, pp. 637–640, 2012.
19. Y. Zhao, Y. Liu, and Z. Zeng, "Using region-based saliency for 3d interest points detection.," in *CAIP (2)*, pp. 108–116, 2013.
20. M. Elad, "Retinex by two bilateral filters," in *Proceedings of the 5th International Conference on Scale Space and PDE Methods in Computer Vision*, *Scale-Space'05*, pp. 217–229, Springer-Verlag, (Berlin, Heidelberg), 2005.
21. R. Song, Y. Liu, R. R. Martin, and P. L. Rosin, "Mesh saliency via spectral processing," *ACM Trans. Graph.* **33**(1), p. 6, 2014.
22. S. Coren, L. M. Ward, and J. T. Enns, *Sensation and perception*, Wiley, 2003.
23. H. Hoppe, T. DeRose, T. Duchamp, J. McDonald, and W. Stuetzle, "Surface reconstruction from unorganized points," *SIGGRAPH Comput. Graph.* **26**(2), pp. 71–78, 1992.
24. J. Henderson, C. Williams, and R. Falk, "Eye movements are functional during face learning," *Memory and cognition* **33**(1), pp. 98–106, 2005.
25. M. Garland and P. S. Heckbert, "Surface simplification using quadric error metrics," in *Proceedings of the 24th Annual Conference on Computer Graphics and Interactive Techniques*, *SIGGRAPH '97*, pp. 209–216, ACM Press/Addison-Wesley Publishing Co., (New York, NY, USA), 1997.